Robust Target Detection and Estimation for Airborne STAP Radar with Arbitrary Array Errors and Target Uncertainty

JIANXIN WU[1], YANG ZHAO[2], CHANGXIAN LI[3], AND PENG SHEN[2]

[1]School of Electronics and Communication Engineering, Sun Yat-sen University, Guangzhou 510275, China
[2]National Laboratory of Radar Signal Processing, Xidian University, Xi'an 710071, China
[3]Chaoyue Digital Control, Jinan 250000, China

Corresponding author: Jianxin Wu (email: wujx65@mail.sysu.edu.cn) and Yang Zhao(email: yzhao_97@stu.xidian.edu.cn)

ABSTRACT In the presence of arbitrary array errors and angle mismatch, performance on target detection and angle estimation will be degraded due to steering vector mismatch. Thus, a robust target detection and estimation algorithm for airborne STAP radar is developed. First, utilizing the spatial-temporal coupling property of the ground clutter, array steering vectors are well estimated by fine Doppler localization of the mainlobe clutter. Then, the robust subspace detector spanned by these estimated array steering vectors is developed, which can improve the detection performance for the targets not located in the look direction. Finally, target angle estimation using subspace coefficients, which implements the ML estimator in a reduced-dimensional version, is presented to reduce the computational complexity of the ML estimator. Numerical examples are given to demonstrate the effectiveness of the presented algorithm.

INDEX TERMS Airborne radar, arbitrary array error, clutter suppression, space time adaptive processing.

I. INTRODUCTION

The ground clutter seen by an airborne radar is extended in both range and angle. It also is spread over a region in Doppler because of the platform motion. Thus, the interested moving target may be masked by the ground clutter. An efficient way to improve target detection performance in airborne radar is to utilize the space-time adaptive processing (STAP) technique [1]–[6]. Theoretically, the STAP processor under homogeneous clutter environments can obtain optimal target detection performance. However, practical considerations, such as limited number of independent and identically distributed (i.i.d.) samples, and steering vector mismatch induced by either array errors or target angle uncertainty, may severely degrades the STAP performance. Here, only steering vector mismatch is considered.

To reduce performance degradation induced by steering vector mismatch, either array calibration or robust beamforming for airborne STAP radar is required. Array calibration is an important aspect of array processing and a variety of methods are developed. The calibration methods can be mainly divided into two categories: calibration source methods[7] and self-calibration methods[8],[9]. Limited by the large size and the movement of the airborne platform, many array calibration algorithms, especially for calibration source methods, can not be applied to airborne

radar. Besides, array errors are usually time-variant, array error calibration should be carried out once in a while. For airborne radar, a typical array calibration technique is based on the ground clutter, which is widely used for channel calibration and gain-phase calibration [10]-[12]. However, in the presence of the position error and mutual coupling, the array errors are direction-dependent, which means that the array errors in different directions are different. In this case, the array calibration techniques only suitable for gain-phase calibration are not effective any more. Consequently, a few robust array signal processing methods[13,14] for unknown mutual coupling are developed, which utilize the properties of mutual coupling for some special arrays, such as uniform linear array[13] or uniform circular array[14]. If accurate array steering vectors are unavailable, we can model steering vector mismatch as a random vector with a typical distribution, such as multivariate complex Gaussian distribution. In this case, many robust algorithms[15]-[20] against steering vector mismatch in statistical sense can be employed for target detection. Additionally, the classical methods for target angle estimation are the ML method[21] and the adaptive monopulse method[22], where the ML method requires all accurate steering vectors in the mainbeam in order to evaluate all likelihood function values, and the adaptive monopulse method also requires all accurate steering vectors in order to form the adaptive

monopulse curve. Thus, it is necessary to estimate all real steering vectors in the mainbeam. Besides, due to target uncertainty, a target can appear in any direction of the mainbeam. Although multiple overlapped spatial beams can be employed to cover the entire mainbeam, it causes high computational complexity especially in the detection stage. In order to reduce the complexity, the STAP processor generally uses single spatial beam to cover the mainbeam. In this case, target angle mismatch often happened. Although the SNR loss induced by angle mismatch is usually less than 3dB, this SNR loss becomes large when the mainlobe clutter is presented in the STAP filter. Hence, target angle mismatch should be taken into account especially in the mainlobe clutter region (which is associated with the slow moving target case).

In this paper, a robust target detection and estimation algorithm for airborne STAP radar is developed against steering vector mismatch. Utilizing the spatial-temporal coupling property of the ground clutter, array steering vectors in the mainbeam are first estimated by fine Doppler localization. To overcome the problem of target angle mismatch with the look direction, the subspace detector spanned by the mainlobe low-rank subspace derived from the estimated steering vectors is developed. Finally, target angle estimation using subspace coefficients which implements the ML estimator in a reduced-dimensional version is given. Numerical examples are given to demonstrate the effectiveness of the presented technique. The main contributions of the paper are summarized as follows.

(1) Steering vector estimation for arbitrary array error is developed, which is based on the spatial-temporal coupling property of airborne radar clutter. Relative to the most existed array calibrated methods, which are developed based on a part of error models, the developed method can handle the arbitrary array errors and is free of the array error model, and thus performance degradation induced by model mismatch is avoided.

(2) A robust subspace detector without the assumption on the statistical model of steering vector mismatch is developed. Unlike the robust subspace detectors in [15-20], which assumed that the actual steering vector is randomly located in the conic area of the presumed steering vector, the presented subspace detector assumed that the actual steering vector is an unknown constant vector, rather than a random vector. Thus, the presented subspace detector can obtain better performance than those subspace detectors based on the statistical assumption on steering vector mismatch.

(3) Fast realization of angle estimation compatible with the subspace detector is developed. Angle estimation can be realized only by a low-dimensional subspace coefficients search. Compared to the full-dimensional search, the complexity can be greatly reduced.

The remainder of this paper is organized as follows:

Section II introduces the signal model and the conventional STAP-AMF detector. A robust target detection and parameter estimation algorithm is developed in Section III. Section IV presents numerical examples to evaluate the performance of the presented algorithm. The final conclusion is then discussed in Section V.

II. SIGNAL MODEL

Consider an airborne sidelooking radar with N subarrays and suppose a coherent burst of M pulses are transmitted. Let x_{nml} denote the received data at the nth subarray, mth pulse, and lth range gate, and

$$\mathbf{x}_l = \left[x_{11l}, x_{21l}, ..., x_{N1l}, x_{12l}, x_{22l}, ..., x_{N2l}, ..., x_{1Ml}, x_{2Ml}, ...x_{NMl}\right]^{\mathrm{T}}$$

denote the $NM \times 1$ received data snapshot. In the absence of the target signal, the data snapshot consists of the clutter and noise components, which can be modeled as[2]

$$\mathbf{x}_l = \sum_{i=1}^{N_c} \alpha_{li} \left(\mathbf{b}(\omega_i) \otimes \mathbf{a}(\vartheta_i)\right) + \mathbf{n}_l \quad (1)$$

where N_c is the number of clutter patches, α_{li}, $\omega_i = \dfrac{2v}{\lambda f_r}\cos\phi_i$, and $\vartheta_i = \dfrac{d}{\lambda}\cos\phi_i$ are the complex amplitude, the normalized Doppler frequency and the normalized spatial frequency of the ith clutter patch at the lth range bin, respectively. v is the velocity of the platform, λ is the wavelength, f_r is the pulse repetition frequency (PRF), d is the element spacing, ϕ_i is the antenna cone angle of the ith clutter patch. $\mathbf{n}_l$ is the noise vector obeying the complex Gaussian distribution with zero mean and the covariance matrix $\mathbf{R}_n$. Additionally,

$$\mathbf{b}(\omega_i) = \left[1 \quad \exp(j2\pi\omega_i) \quad \cdots \quad \exp(j2\pi(M-1)\omega_i)\right]^{\mathrm{T}} \in C^{M\times 1}$$

is a temporal steering vector, $\mathbf{a}(\vartheta_i) = \bar{\mathbf{a}}(\vartheta_i) \odot \mathbf{e}(\vartheta_i) \in C^{N\times 1}$ is a spatial steering vector with arbitrary array error, $\bar{\mathbf{a}}(\vartheta_i) = \left[1 \quad \exp(j2\pi\vartheta_i) \quad \cdots \quad \exp(j2\pi(N-1)\vartheta_i)\right]^{\mathrm{T}}$ is an assumed spatial steering vector, and $\mathbf{e}(\vartheta_i)$ denotes the angle-dependent array error.

Due to the need for lower computational complexity and fewer secondary data, the temporal reduced dimensional transform, such as the FA(Factored Algorithm)method and the EFA(Extended Factored Algorithm) method[1], is first used before adaptive processing. Here the EFA method is considered. The data vector associated with the mth Doppler filter can be represented by $\mathbf{x}_{Tml} = \mathbf{T}_m^{\mathrm{H}}\mathbf{x}_l$, where $\mathbf{T}_m = \mathbf{F}_m \otimes \mathbf{I}_N$ is the reduced dimensional matrix of the EFA processor, $\mathbf{I}_N$ is the identity matrix, $\mathbf{F}_m = \left[\mathbf{f}_{m-1} \quad \mathbf{f}_m \quad \mathbf{f}_{m+1}\right]$ is the temporal reduced-dimensional matrix, and

$$\mathbf{f}_m = \left[1 \quad \exp(j2\pi m/M) \quad \cdots \quad \exp(j2\pi m(M-1)/M)\right]^{\mathrm{T}}$$

is the mth Doppler filter coefficient vector.

Two hypotheses are postulated as

$$\begin{cases} H_0 : \mathbf{x}_{\mathrm{T}ml_0} = \mathbf{x}_{\mathrm{T}m0} \\ H_1 : \mathbf{x}_{\mathrm{T}ml_0} = \alpha \mathbf{v}(\omega_{\mathrm{t}}, \vartheta_{\mathrm{t}}) + \mathbf{x}_{\mathrm{T}m0} \end{cases} \quad (2)$$

where l_0 denotes the range cell under test (CUT), $\mathbf{x}_{\mathrm{T}m0} \in C^{3N \times 1}$ is a clutter-plus-noise vector obeying the complex Gaussian distribution with zero mean and the covariance matrix $\mathbf{R}$, α is the fixed but unknown target amplitude,

$$\mathbf{v}(\omega_{\mathrm{t}}, \vartheta_{\mathrm{t}}) = \mathbf{T}_m^{\mathrm{H}}(\mathbf{b}(\omega_{\mathrm{t}}) \otimes \mathbf{a}(\vartheta_{\mathrm{t}})) = [\mathbf{s}_{mt} \otimes \mathbf{a}(\vartheta_{\mathrm{t}})] \in C^{3N \times 1}$$

is a reduced-dimensional target steering vector with the spatial frequency of ϑ_{t} and the Doppler frequency of ω_{t}, and $\mathbf{s}_{mt} = \mathbf{F}_m^{\mathrm{H}} \mathbf{b}(\omega_{\mathrm{t}})$.

The detection problem is formulated as a dual hypothesis testing problem given in (2). This problem can be solved by the adaptive matched filter (AMF) detector[23], whose test statistic is of the form

$$\Lambda_{\mathrm{AMF}} = \frac{\left| \mathbf{v}^{\mathrm{H}}(\omega_{m0}, \vartheta_0) \hat{\mathbf{R}}^{-1} \mathbf{x}_{\mathrm{T}ml_0} \right|^2}{\mathbf{v}^{\mathrm{H}}(\omega_{m0}, \vartheta_0) \hat{\mathbf{R}}^{-1} \mathbf{v}(\omega_{m0}, \vartheta_0)} \quad (3)$$

where $\mathbf{v}(\omega_{m0}, \vartheta_0) = \mathbf{T}_m^{\mathrm{H}}(\mathbf{b}(\omega_{m0}) \otimes \overline{\mathbf{a}}(\vartheta_0))$ is the assumed steering vector, $\hat{\mathbf{R}} = \frac{1}{L} \sum_{l=1,l \neq l_0}^{L} \mathbf{x}_{\mathrm{T}ml} \mathbf{x}_{\mathrm{T}ml}^{\mathrm{H}}$ is the sample covariance matrix, ϑ_0 is the normalized spatial frequency of the look direction and ω_{m0} is the normalized Doppler frequency associated with the center of the mth Doppler filter. In practice, the AMF detector can be considered as the cell averaging constant false alarm rate (CA-CFAR) detector of the STAP filter output, which is given by

$$\begin{aligned} \Lambda_{\mathrm{AMF}} &= \frac{\left| \mathbf{w}^{\mathrm{H}}(\omega_{m0}, \vartheta_0) \mathbf{x}_{\mathrm{T}ml_0} \right|^2}{\mathbf{w}^{\mathrm{H}}(\omega_{m0}, \vartheta_0) \frac{1}{L} \sum_{l=1}^{L} \mathbf{x}_{\mathrm{T}ml} \mathbf{x}_{\mathrm{T}ml}^{\mathrm{H}} \mathbf{w}(\omega_{m0}, \vartheta_0)} \\ &= \frac{\left| y_{\mathrm{T}l_0} \right|^2}{\frac{1}{L} \sum_{l=1,l \neq l_0}^{L} \left| y_l \right|^2} \end{aligned} \quad (4)$$

where $\mathbf{w}(\omega_{m0}, \vartheta_0) = \hat{\mathbf{R}}^{-1} \mathbf{v}(\omega_{m0}, \vartheta_0)$ is the weight vector of the STAP filter. It means that target detection can be realized only in the STAP sum channel by performing CA-CFAR detection. However, if the target angle deviates from the look direction, the STAP output will decrease with the angle offset increasing. In this case, the target detection performance is degraded. To improve the robustness on detecting all possible mainlobe targets, more STAP filter outputs should be employed. Similar cases will happen when the target Doppler frequency deviates from the center of the Doppler filter.

Once target detection is finished, target parameter estimation is another task for an airborne STAP radar,

which can be implemented by the adaptive monopulse technique or the maximum likelihood technique. However, in the presence of array errors, the assumed monpulse curve will be deviated from the true monopulse curve, and thus performance degradation on angle estimation occurs. Similarly, in the presence of array errors, there exists a mismatch between the assumed steering vectors and the true steering vectors, and thus the performance of ML estimation will be degraded. To improve the robustness against arbitrary array errors, the true steering vectors should be estimated in advanced.

III. ROBUST TARGET DETECTION AND TARGET PARAMETER ESTIMATION

To overcome steering vector mismatch resulted from array errors and arbitrariness of the target direction, robust target detection and estimation using estimated steering vectors and the subspace detector is developed.

A. STEERING VECTORS ESTIMATION

From (1), we know that the clutter-plus-noise component can be written as

$$\mathbf{x}_l = \sum_{i=1}^{N_c} \alpha_{li} \mathbf{b}(\omega_i) \otimes \mathbf{a}(\vartheta_i) + \mathbf{n}_l \quad (5)$$

According to the definitions of ω_i and ϑ_i given in (1), the relationship of the two frequencies can be represented by

$$\omega_i = \frac{2v}{df_r} \vartheta_i \quad i = 1, 2, ..., N_c \quad (6)$$

It means that clutter patches can be localized either by a spatial filter or by a Doppler filter. Since the error level in time domain is much lower than that in spatial domain, the ultra-low sidelobe of a Doppler filter is more feasible than that of a spatial filter. Thus, it is preferred to use Doppler localization to realize clutter localization. Doppler localization can be realized by Doppler filtering, where the mth Doppler filter output is given by

$$\begin{aligned} \mathbf{y}_{ml} &= (\mathbf{f}_m \otimes \mathbf{I}_N)^{\mathrm{H}} \mathbf{x}_l \\ &= \sum_{i=1}^{N_c} \alpha_{li} (\mathbf{f}_m \otimes \mathbf{I}_N)^{\mathrm{H}} (\mathbf{b}(\omega_i) \otimes \mathbf{a}(\vartheta_i)) + (\mathbf{f}_m \otimes \mathbf{I}_N)^{\mathrm{H}} \mathbf{n}_l \\ &= \sum_{i=1}^{N_c} \alpha_{li} \, psf(\omega_m - \omega_i) \mathbf{a}(\vartheta_i) + \overline{\mathbf{n}}_l \end{aligned}$$

$$(7)$$

where $psf(\omega_m - \omega_i) = \mathbf{f}_m^{\mathrm{H}} \mathbf{b}(\omega_i)$ is the low-pass filter response with the passband of

$$\left| \omega_i - \omega_m \right| \leq \frac{1}{2M} \quad (8)$$

and $\overline{\mathbf{n}}_l = (\mathbf{f}_m \otimes \mathbf{I}_N)^{\mathrm{H}} \mathbf{n}_l$ is the additive Gaussian noise. According to the Doppler frequency passband of the mth Doppler filter, we can obtain the associated spatial frequency passband of the clutter component by substituting (6) into (8)

$$\frac{df_r}{2v}\omega_m - \frac{df_r}{4Mv} \le \vartheta_i \le \frac{df_r}{2v}\omega_m + \frac{df_r}{4Mv} \qquad (9)$$

The width of the spatial frequency passband is

$$\Delta = \frac{df_r}{2Mv} \qquad (10)$$

Since the gain of the stopband of a Doppler filter is much less than that of the passband, it is reasonable to only take the components in the passband into account and (7) can be simplified to

$$\mathbf{y}_{ml} = \sum_{i=N_m}^{\bar{N}_m} \bar{\alpha}_{li}\mathbf{a}(\vartheta_i) + \bar{\mathbf{n}}_l \qquad (11)$$

where N_m and $\bar{N}_m$ are the bounded clutter indexes of the mth Doppler filter, and $\bar{\alpha}_{li} = \alpha_{li}\,psf(\omega_m - \omega_i)$. Similar to the Doppler beam sharpening (DBS) radar, we define the sharpening ratio as

$$g = \frac{\theta_w}{\Delta} = \frac{2Mv}{Ndf_r} \qquad (12)$$

where θ_w is the mainlobe beamwidth.
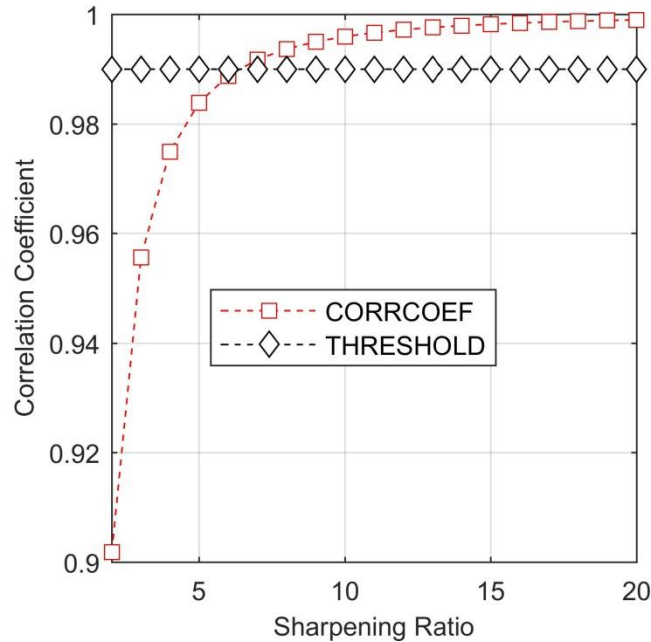
FIGURE 1. Correlation coefficient of $\mathbf{a}(\vartheta_i)$ and $\mathbf{a}(\vartheta_i + \Delta)$ versus the sharpening ratio.

Fig.1 demonstrates the correlation coefficient of $\mathbf{a}(\vartheta_i)$ and $\mathbf{a}(\vartheta_i + \Delta)$ versus the sharpening ratio, where the marker of diamond denotes the threshold value of the correlation coefficient. It is shown that as long as the sharpening ratio is larger than 8, the correlation coefficient of $\mathbf{a}(\vartheta_i)$ and $\mathbf{a}(\vartheta_i + \Delta)$ can be guaranteed to be greater than 0.99. Under this condition, $\mathbf{a}(\vartheta_i + \Delta)$ can be well approximated by $\mathbf{a}(\vartheta_i)$, that is, $\mathbf{a}(\vartheta_i + \Delta) \approx \mathbf{a}(\vartheta_i)$. To get high sharpening ratio, long coherent processing interval (CPI) or fast platform velocity are desired.

Under the high sharpening ratio case, (11) can be simplified as

$$\mathbf{y}_{ml} = \beta_{lm}\mathbf{a}(\vartheta_m) + \bar{\mathbf{n}}_l \qquad (13)$$

where $\beta_{lm} = \sum_{i=N_m}^{\bar{N}_m} \bar{\alpha}_{li}$. Finally, to reduce the adverse effects of $\bar{\mathbf{n}}_l$, multiple i.i.d. range bins are averaged for estimating $\mathbf{a}(\vartheta_m)$. According to the model given in (13), the covariance matrix of $\mathbf{y}_{ml}$ is given by

$$\mathbf{R}_{ml} = E\left[\mathbf{y}_{ml}\mathbf{y}_{ml}^{\mathrm{H}}\right] = \sigma_{clm}^2\mathbf{a}(\vartheta_m)\mathbf{a}^{\mathrm{H}}(\vartheta_m) + \sigma_n^2\mathbf{I}_N \qquad (14)$$

where $\sigma_{clm}^2 = E\left[|\beta_{lm}|^2\right]$, $E\left[\bar{\mathbf{n}}_l\bar{\mathbf{n}}_l^{\mathrm{H}}\right] = \sigma_n^2\mathbf{I}_N$ and σ_n^2 is the noise power. As we know, the clairvoyant covariance matrix of $\mathbf{R}_{ml}$ is unknown and must be estimated by multiple i.i.d. range bins in a real environment

$$\hat{\mathbf{R}}_{ml_0} = \frac{1}{L}\sum_{l=1}^{L}\mathbf{y}_{ml}\mathbf{y}_{ml}^{\mathrm{H}} \qquad (15)$$

where $\mathbf{y}_{ml}$ is the lth i.i.d. range bin of $\mathbf{y}_m$.

For the mainlobe clutter, the clutter-to-noise (CNR) ratio, which is defined as $\mathrm{CNR} = \frac{\sigma_{cm}^2}{\sigma_n^2}$, is much larger than 1. Thus, it is valid to suppose the number of large eigenvalues of $\hat{\mathbf{R}}_m$ is 1 and $\mathbf{a}(\vartheta_m)$ can be obtained by the eigenvector associated with the largest eigenvalue.

In a real environment, adjacent range bins perhaps include some strong moving targets or other unwanted components. Thus, secondary data selection is usually necessary. Classical data selection methods include the generalized inner product (GIP) statistic, a combination of the six methods including fast maximum likelihood algorithm (FML), reiterative censoring, adaptive power residue (APR) metric, concurrent block processing, two weight method, and adaptive coherence estimate (FRACTRA)[24], which are widely used in STAP, can be used here. However, these methods require high computational burden due to the matrix inversion operation. To reduce the computational complexity, we use both the inner product (IP) statistic and the correlation coefficient to select secondary data, where the IP statistic is defined as

$$\gamma_l = \left|\mathbf{a}^{\mathrm{H}}(\vartheta_m)\mathbf{y}_{ml}\right|^2 \qquad (16)$$

and the correlation coefficient (CC) is defined as

$$\mu_l = \frac{\left|\mathbf{a}^{\mathrm{H}}(\vartheta_m)\mathbf{y}_{ml}\right|^2}{\mathbf{a}^{\mathrm{H}}(\vartheta_m)\mathbf{a}(\vartheta_m)\cdot\mathbf{y}_{ml}^{\mathrm{H}}\mathbf{y}_{ml}} \qquad (17)$$

From the definition of the IP statistic given in (16), we know that the IP statistic is dependent on both the amplitude and the direction of $\mathbf{y}_{ml}$. Consequently, the IP statistic may be still large as long as the amplitude of $\mathbf{y}_{ml}$ is large, no matter whether $\mathbf{y}_{ml}$ comes from the direction of ϑ_m or not. Strong outliers, such as strong targets and strong jammers, whose directions are different from ϑ_m, also have large IP values. Thus, it is not effective to select

secondary data only using the IP statistic and a combined statistic is desired. From the definition of the CC given in (17), we know that if $\mathbf{y}_{ml}$ comes from the direction of ϑ_m, then the CC is large. Thus, the CC can be considered as a performance metric for direction matching.

The basic idea of the combined statistic of IP and CC can be summarized as follows. First, the IP is used to pick out the strongest range bins which may be the strong clutter or the strong outliers. Second, the CC is employed to kick out the possible outliers. Thereafter, the strong clutter can be well preserved and the outliers are removed by the combined statistic.

The procedures of the presented method are summarized as follows:

Step 1: Compute the clutter spatial steering vector $\mathbf{a}(\vartheta_m)$ associated with the mth Doppler filter according to (5).

Step 2: Compute the IP and the CC of $\mathbf{a}(\vartheta_m)$ and $\mathbf{y}_{ml}$ for all range bins according to (16) and (17).

Step 3: Find I maximal values of γ_l among all L range bins, i.e., $\left\{l_1, l_2, ..., l_{L_I}\right\} = \arg\max_{l}\left\{\gamma_l\right\}, l = 1, 2, ..., L$

Step 4: Find K maximal values of μ_l among the I range bins given in step 3, i.e.,
$$\left\{l_1, l_2, ..., l_{L_K}\right\} = \arg\max_{l}\left\{\mu_l\right\}, l = l_1, l_2, ..., l_{L_I}$$

Step 5: Construct the covariance matrix $\hat{\mathbf{R}}_m$ given in (15) using K range bins given in step 4.

Step 6: Perform singular value decomposition (SVD) on $\hat{\mathbf{R}}_m$ to find the eigenvector associated with the largest eigenvalue, which is considered as the estimate of $\mathbf{a}(\vartheta_m)$.

Step 7: Go to step 1 until all Doppler filters in the mainlobe clutter region are processed.

B. ROBUST DETECTION AGAINST ARBITRARY ARRAY ERRORS AND TARGET UNCERTAINTY

Due to target uncertainty, a target will emerge in any direction of the mainbeam. If a target emerges at the edge of the mainbeam, then the gain loss of this target occurs, and the detection performance is degraded. To improve the detection performance at the edge of the mainbeam, a robust target detection method which is based on the subspace detector[24-26] is developed.

Consider all possible targets in the mainbeam, (2) can be rewritten as

$$\begin{cases} H_0 : \mathbf{x}_{Tml_0} = \mathbf{x}_{Tm0} \\ H_1 : \mathbf{x}_{Tml_0} = \alpha\mathbf{v}(\omega_t, \vartheta_t) + \mathbf{x}_{Tm0} \end{cases} \quad \vartheta_0 - \frac{\Delta}{2} \le \vartheta_t \le \vartheta_0 + \frac{\Delta}{2} \quad (18)$$

where $\mathbf{x}_{Tm0} \in C^{3N \times 1}$ is a clutter-plus-noise vector obeying the complex Gaussian distribution with zero mean and the covariance matrix $\mathbf{R}$, α is a fixed but unknown target amplitude, ω_t is the target Doppler frequency, ϑ_0 is the spatial frequency of the look direction, and Δ is the beamwidth. Since the steering vectors in the beamwidth is

highly correlated, the steering matrix $\mathbf{V} = \begin{bmatrix} \mathbf{v}(\omega_t, \vartheta_1) & \mathbf{v}(\omega_t, \vartheta_2) & \cdots & \mathbf{v}(\omega_t, \vartheta_{\bar{N}}) \end{bmatrix}$, which is composed of all steering vectors in the mainbeam, is low-rank. It means that $\mathbf{V}$ can be written in the form of low-rank SVD

$$\mathbf{V} = \mathbf{U}_s \mathbf{\Lambda}_s \mathbf{\Phi}_s^H \quad (19)$$

where $\mathbf{U}_s \in C^{Q \times P}$, $\mathbf{\Lambda}_s \in C^{P \times P}$, $\mathbf{\Phi}_s \in C^{\bar{N} \times P}$, and P is the dimension of the low-rank subspace. Then, the nth column vector of $\mathbf{V}$, $\mathbf{v}(\omega_t, \vartheta_n)$, can be represented as

$$\mathbf{v}(\omega_t, \vartheta_n) \approx \mathbf{U}_s \boldsymbol{\rho}(\vartheta_n) \quad (20)$$

where $\boldsymbol{\rho}(\vartheta_n) = \left(\mathbf{U}_s^H \mathbf{U}_s\right)^{-1} \mathbf{U}_s^H \mathbf{v}(\omega_t, \vartheta_n)$.

In this case, (18) can be rewritten as

$$\begin{cases} H_0 : \mathbf{x}_{Tml_0} = \mathbf{x}_{Tm0} \\ H_1 : \mathbf{x}_{Tml_0} = \mathbf{U}_s \bar{\boldsymbol{\rho}}_n + \mathbf{x}_{Tm0} \end{cases} \quad (21)$$

where $\bar{\boldsymbol{\rho}}_n = \alpha\boldsymbol{\rho}(\vartheta_n)$. The generalized likelihood ratio test (GLRT)[26] of (21) can be written as

$$\Lambda = \max_{\bar{\boldsymbol{\rho}}_n} \bar{\Lambda}(\bar{\boldsymbol{\rho}}_n) \underset{H_0}{\overset{H_1}{\gtrless}} \gamma \quad (22)$$

$$\bar{\Lambda}(\bar{\boldsymbol{\rho}}_n) = \frac{f_{\mathbf{x}_{Tm}|H_1}\left(\mathbf{x}_{Tml_0}; \bar{\boldsymbol{\rho}}_n \mid H_1\right)}{f_{\mathbf{x}_{Tm}|H_0}\left(\mathbf{x}_{Tml_0} \mid H_0\right)} \quad (23)$$

where γ is the threshold determined by the false alarm rate. According to the statistical model assumption made in (18), the complex multivariate Gaussian density functions under H_1 and H_0 are given by

$$f_{\mathbf{x}_{Tm}|H_1}\left(\mathbf{x}_{Tml_0}; \bar{\boldsymbol{\rho}}_n \mid H_1\right) = \frac{1}{(2\pi)^{\frac{3N}{2}}|\mathbf{R}|^{\frac{1}{2}}} e^{-\left(\mathbf{x}_{Tml_0} - \mathbf{U}_s\bar{\boldsymbol{\rho}}_n\right)^H \mathbf{R}^{-1}\left(\mathbf{x}_{Tml_0} - \mathbf{U}_s\bar{\boldsymbol{\rho}}_n\right)}$$

$$(24)$$

$$f_{\mathbf{x}_{Tm}|H_0}\left(\mathbf{x}_{Tml_0} \mid H_0\right) = \frac{1}{(2\pi)^{\frac{3N}{2}}|\mathbf{R}|^{\frac{1}{2}}} e^{-\mathbf{x}_{Tml_0}^H \mathbf{R}^{-1}\mathbf{x}_{Tml_0}} \quad (25)$$

Substituting the complex multivariate Gaussian density functions into (23) and canceling common terms yields

$$\bar{\Lambda}(\bar{\boldsymbol{\rho}}_n) = e^{-\left(\mathbf{x}_{Tml_0} - \mathbf{U}_s\bar{\boldsymbol{\rho}}_n\right)^H \mathbf{R}^{-1}\left(\mathbf{x}_{Tml_0} - \mathbf{U}_s\bar{\boldsymbol{\rho}}_n\right) + \mathbf{x}_{Tml_0}^H \mathbf{R}^{-1}\mathbf{x}_{Tml_0}} \quad (26)$$

The logarithm version of (26) is simplified to

$$\log\bar{\Lambda}(\bar{\boldsymbol{\rho}}_n) = 2\mathrm{Re}\left(\bar{\boldsymbol{\rho}}_n^H \mathbf{U}_s^H \mathbf{R}^{-1}\mathbf{x}_{Tml_0}\right) - \bar{\boldsymbol{\rho}}_n^H \mathbf{U}_s^H \mathbf{R}^{-1}\mathbf{U}_s\bar{\boldsymbol{\rho}}_n \quad (27)$$

and the logarithm version of the GLRT in (22) is

$$\log\Lambda = \max_{\bar{\boldsymbol{\rho}}_n} \log\bar{\Lambda}(\bar{\boldsymbol{\rho}}_n) \underset{H_0}{\overset{H_1}{\gtrless}} \beta \quad (28)$$

where $\beta = \log\gamma$.

Maximizing (27) with respect to the unknown quantity $\bar{\boldsymbol{\rho}}_n$ yields

$$\bar{\boldsymbol{\rho}}_n = \left(\mathbf{U}_s^{\mathrm{H}}\mathbf{R}^{-1}\mathbf{U}_s\right)^{-1}\mathbf{U}_s^{\mathrm{H}}\mathbf{R}^{-1}\mathbf{x}_{\mathrm{T}ml_0} \qquad (29)$$

Substituting (29) into (28) yields

$$\log\Lambda = \mathbf{x}_{\mathrm{T}ml_0}^{\mathrm{H}}\mathbf{R}^{-1}\mathbf{U}_s\left(\mathbf{U}_s^{\mathrm{H}}\mathbf{R}^{-1}\mathbf{U}_s\right)^{-1}\mathbf{U}_s^{\mathrm{H}}\mathbf{R}^{-1}\mathbf{x}_{\mathrm{T}ml_0} \underset{H_0}{\overset{H_1}{\gtrless}} \beta \qquad (30)$$

Since the true covariance matrix is unknown, it is usually replaced by the sample covariance matrix, i.e.,

$$\hat{\mathbf{R}} = \frac{1}{L}\sum_{l=1,l\neq l_0}^{L}\mathbf{x}_{\mathrm{T}ml}\mathbf{x}_{\mathrm{T}ml}^{\mathrm{H}} \qquad (31)$$

where $\mathbf{x}_{\mathrm{T}ml}$ is the data snapshot of the lth i.i.d. range bin. Define $\mathbf{w}_p = \hat{\mathbf{R}}^{-1}\mathbf{u}_{sp}$ as the pth weight vector of STAP filters and $z_{pl_0} = \mathbf{w}_p^{\mathrm{H}}x_{\mathrm{T}ml_0}$ as the filter output using the pth weight vector, (30) can be rewritten as

$$\log\Lambda = \mathbf{z}_{l_0}^{\mathrm{H}}\mathbf{R}_z^{-1}\mathbf{z}_{l_0} \qquad (32)$$

where $\mathbf{z}_{l_0} = \begin{bmatrix} z_{1l_0} & z_{2l_0} & \cdots & z_{Pl_0} \end{bmatrix}^{\mathrm{T}} = \mathbf{U}_s^{\mathrm{H}}\mathbf{R}^{-1}\mathbf{x}_{\mathrm{T}ml_0}$, and $\mathbf{R}_z = E\left[\mathbf{z}\mathbf{z}^{\mathrm{H}}|H_0\right] = \mathbf{U}_s^{\mathrm{H}}\mathbf{R}^{-1}\mathbf{U}_s$. It means that the subspace detector realizes target energy accumulation using P filter outputs, rather than single filter output.

In practice, the conventional AMF detector given in (3) can also be expressed in a similar form

$$\Lambda_{\mathrm{AMF}} = \frac{\left|\mathbf{v}^{\mathrm{H}}\left(\omega_{m0},\vartheta_{n0}\right)\hat{\mathbf{R}}^{-1}\mathbf{x}_{\mathrm{T}ml_0}\right|^2}{\mathbf{v}^{\mathrm{H}}\left(\omega_{m0},\vartheta_{n0}\right)\hat{\mathbf{R}}^{-1}\mathbf{v}\left(\omega_{m0},\vartheta_{n0}\right)} \qquad (33)$$

$$= z_{l_0}^{\mathrm{H}}R_z^{-1}z_{l_0}$$

where $z_{l_0} = \mathbf{w}_0^{\mathrm{H}}\mathbf{x}_{\mathrm{T}ml_0} = \mathbf{v}^{\mathrm{H}}\left(\omega_{m0},\vartheta_{n0}\right)\hat{\mathbf{R}}^{-1}\mathbf{x}_{\mathrm{T}ml_0}$, and

$$R_z = E\left[z_{l_0}z_{l_0}^{\mathrm{H}}|H_0\right] = \mathbf{v}^{\mathrm{H}}\left(\omega_{m0},\vartheta_{n0}\right)\hat{\mathbf{R}}^{-1}\mathbf{v}\left(\omega_{m0},\vartheta_{n0}\right).$$

Comparing (32) with (33), one can observe that the subspace detector utilizes more dimensions than the conventional AMF detector to improve target accumulation ability when target mismatch occurs.

C. ROBUST TARGET ANGLE ESTIMATION AGAINST ARBITRARY ARRAY ERROR

The ML estimate of target angle is given by[21]

$$\hat{\vartheta}_t = \arg\max_{\vartheta_t} \frac{\left|\mathbf{v}^{\mathrm{H}}\left(\omega_{m0},\vartheta_t\right)\hat{\mathbf{R}}^{-1}\mathbf{x}_{\mathrm{T}ml_0}\right|^2}{\mathbf{v}^{\mathrm{H}}\left(\omega_{m0},\vartheta_t\right)\hat{\mathbf{R}}^{-1}\mathbf{v}\left(\omega_{m0},\vartheta_t\right)} \qquad (34)$$

For brevity, it is assumed that the target Doppler frequency is known since the accuracy on velocity estimation using Doppler filter banks is generally satisfactory in many situations. To guarantee the global optimal solution, fine grid search is usually employed. The computational complexity of the fine grid search method is $9N^2Q + 6NQ$ complex multiplications[21], where Q is the number of grids in the mainbeam. Fortunately, the

steering matrix in the mainbeam is low-rank and $\mathbf{v}\left(\omega_m,\vartheta_t\right)$ can be well approximated by a linear combination of the low-rank subspace, which is similar to (20), that is,

$$\mathbf{v}\left(\omega_{m0},\vartheta_t\right) = \mathbf{U}_s\boldsymbol{\rho}\left(\vartheta_t\right) \qquad (35)$$

Substituting (35) into (34) yields

$$\hat{\vartheta}_t = \arg\max_{\vartheta_t} \frac{\boldsymbol{\rho}^{\mathrm{H}}\left(\vartheta_t\right)\mathbf{U}_s^{\mathrm{H}}\hat{\mathbf{R}}^{-1}\mathbf{x}_{\mathrm{T}ml_0}\mathbf{x}_{\mathrm{T}ml_0}^{\mathrm{H}}\hat{\mathbf{R}}^{-1}\mathbf{U}_s\boldsymbol{\rho}\left(\vartheta_t\right)}{\boldsymbol{\rho}^{\mathrm{H}}\left(\vartheta_t\right)\mathbf{U}_s^{\mathrm{H}}\hat{\mathbf{R}}^{-1}\mathbf{U}_s\boldsymbol{\rho}\left(\vartheta_t\right)} \qquad (36)$$

$$= \arg\max_{\vartheta_t} \frac{\left|\boldsymbol{\rho}^{\mathrm{H}}\left(\vartheta_t\right)\mathbf{z}_{l_0}\right|^2}{\boldsymbol{\rho}^{\mathrm{H}}\left(\vartheta_t\right)\mathbf{R}_z\boldsymbol{\rho}\left(\vartheta_t\right)}$$

By searching the maximum of the cost function over the entire beamwidth, the global optimal solution can be obtained.

The procedures of the reduced dimensional ML estimator are summarized as follows:

Step 1: Compute the pth adaptive weight vector $\mathbf{w}_p$, which requires $\left(3N\right)^2$ complex multiplications;

Step 2: Filter the target data $x_{\mathrm{T}ml_0}$ and P basis $\left\{\mathbf{u}_{s1},...,\mathbf{u}_{sP}\right\}$ with $\mathbf{w}_p$, which requires $3N + 3PN$ complex multiplications;

Step 3: Repeat step1 and step 2 until all P adaptive weight vectors are processed.

Step 4: Given a value of ϑ_t in the mainbeam, compute the concentrated log-likelihood function using (36), which requires $P^2 + 2P$ complex multiplications;

Step 5: Repeat step 4 until the concentrated log-likehood functions for all values of ϑ_t are evaluated.

Step 6: Find the maximum by a sort method.

Thus, the total computational complexity of the presented algorithm is $9N^2P + 9N\left(P^2 + P\right) + \left(P^2 + 2P\right)Q$ complex multiplications. Since the presented method searches the maximum of the log-likelihood function in the entire beamwidth with fine grids, the estimated result can be guaranteed to be global optimal.

Additionally, the adaptive monopulse method is a classical angle estimation method for an adaptive radar. Its computational complexity is $18N^2$ complex multiplications [21]. Although the adaptive monopulse method owns lower computational complexity, it cannot be guaranteed to be global optimal, since it is developed based on the second-order Taylor approximation of the log-likelihood function.

To demonstrate the computational advantage of the presented method over the conventional grid search method, the computational complexity ratio (CCR) relative to the adaptive monopulse method is employed, which is defined as a ratio between the computational complexity of the given method and that of the adaptive monopulse method. Fig.2 shows a comparison on CCR for the three methods. It is observed that the presented method (RD-ML) have lower computational complexity compared to the conventional

grid search method(C-ML). Certainly, the adaptive monopulse method owns the lowest computational complexity among the three methods.
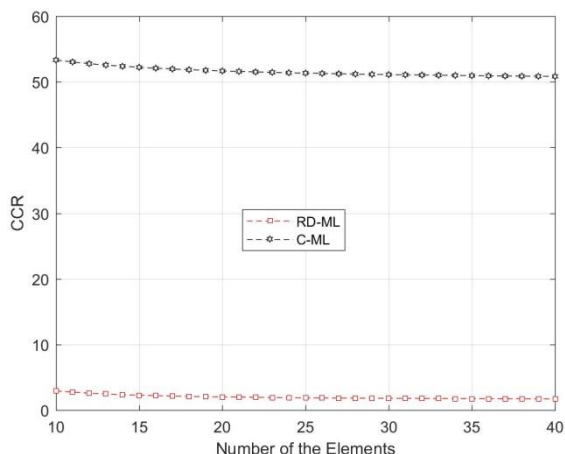

**FIGURE 2.** Comparison on CCR, where P=3, and Q=100.

IV. NUMERICAL EXAMPLES

In this section, numerical examples are given to demonstrate the performance of the developed method. System parameters are listed as follows. The wavelength is 0.5m, the velocity of the platform is 100m/s, the pulse repetition frequency is 1000Hz, the number of coherent pulses is 128, the number of linear array elements is 8, the element spacing is half-wavelength, the beamwidth is 12.5°, and the look direction is steered to the boresight angle of 0°. The first example shows the accuracy on steering vector estimation under arbitrary array errors. The second example demonstrates detection performance as a function of SNR and target angle. The third example gives angle estimation performance as a function of target angle.

A. STEERING VECTOR ESTIMATION PERFORMANCE

According to the system parameters, the Doppler bandwidth of the mainlobe clutter is 100Hz, and the Doppler resolution is 7.8Hz. Thus, the number of Doppler filters occupied by the mainlobe clutter, i.e., the sharpening ratio, is 13, and the associated Doppler channel indexes are from 59 to 71. Steering vector estimation uses the method given in section 3.A. In Fig.3, PD processing results and the interferometry phase of adjacent elements are given. It is shown that the interferometry phase linearly varies with the Doppler index in the clutter region, which is accord with the relationship between the clutter spatial frequency and the clutter Doppler frequency. Moreover, the interferometry phase of the clutter with high CNR has better performance than that of the clutter with low CNR. Thus, secondary data selection is required for improved performance on steering vector estimation. In Fig.4, estimated steering vectors and true steering vectors of all Doppler channels in the mainbeam are given. It is shown that the estimated steering vectors are very close to the true steering vectors for all Doppler channels. For clarity, Fig.5

demonstrates the amplitudes and phases of the actual steering vector, the estimated steering vector and the assumed steering vector of the 65th Doppler channel. It is shown that the estimated steering vector is much closer to the actual steering vector than the assumed steering vector.
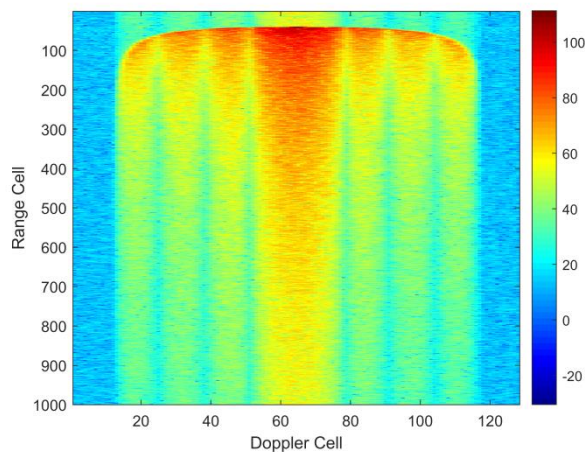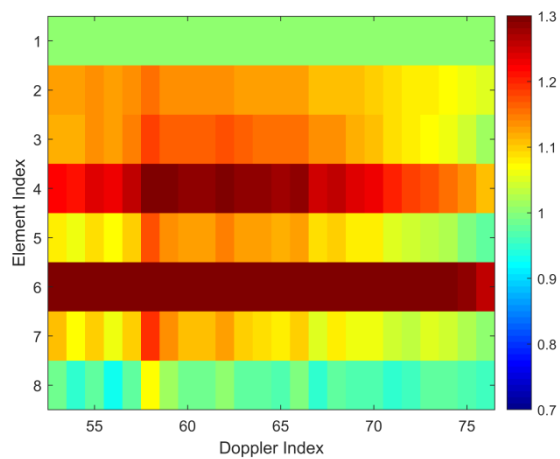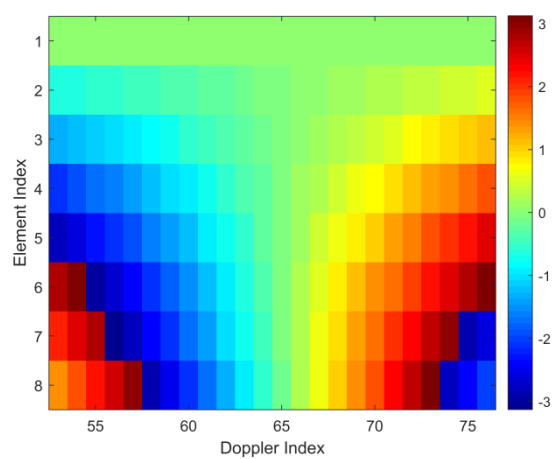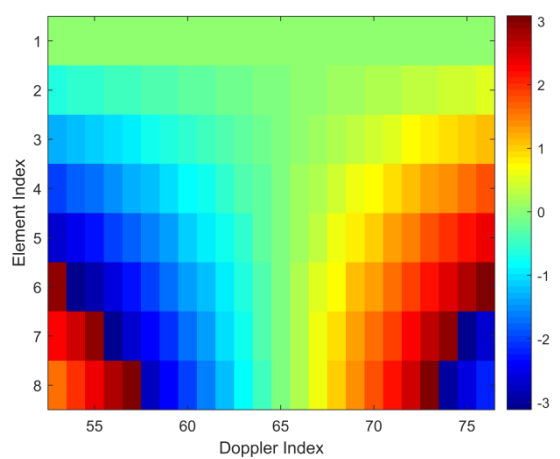

(a)
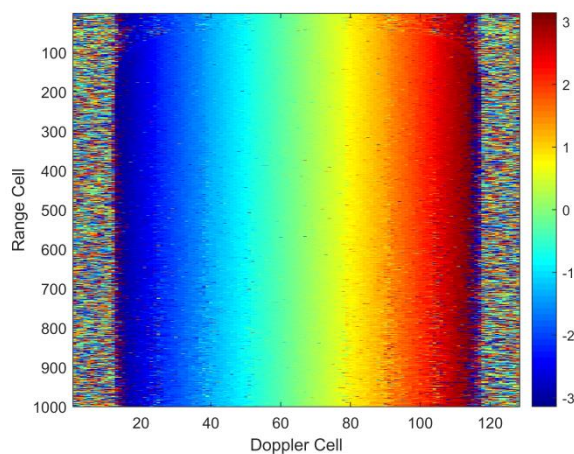
(b)

FIGURE 3. Results of adjacent elements. (a) PD processing, (b) Interferometry phase.
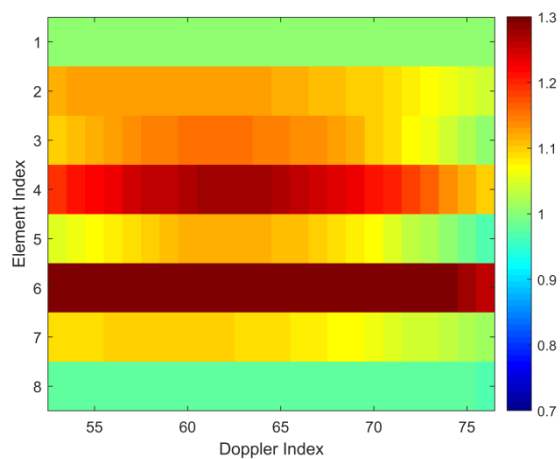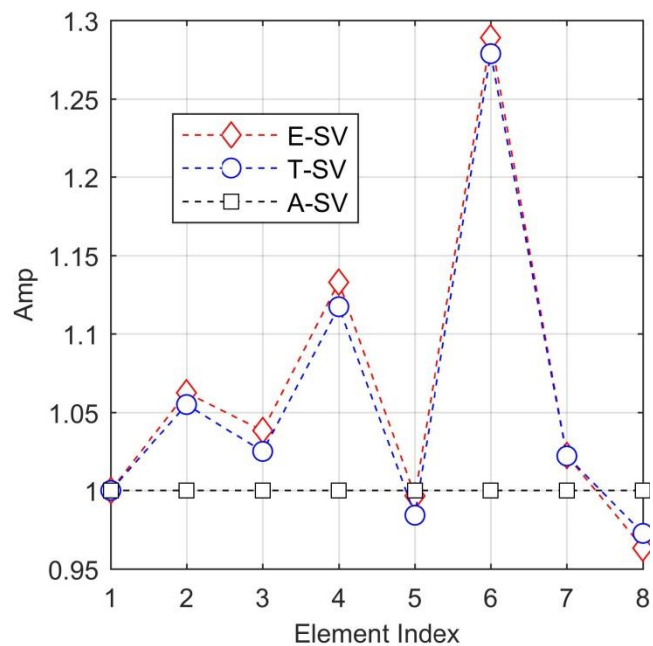
(a)

(d)

FIGURE 4. Steering vector estimation results of the mainbeam. (a) Amplitude of the estimated steering vector, (b) Phase of the estimated steering vector, (c) Amplitude of the true steering vector, (d) Phase of the true steering vector.
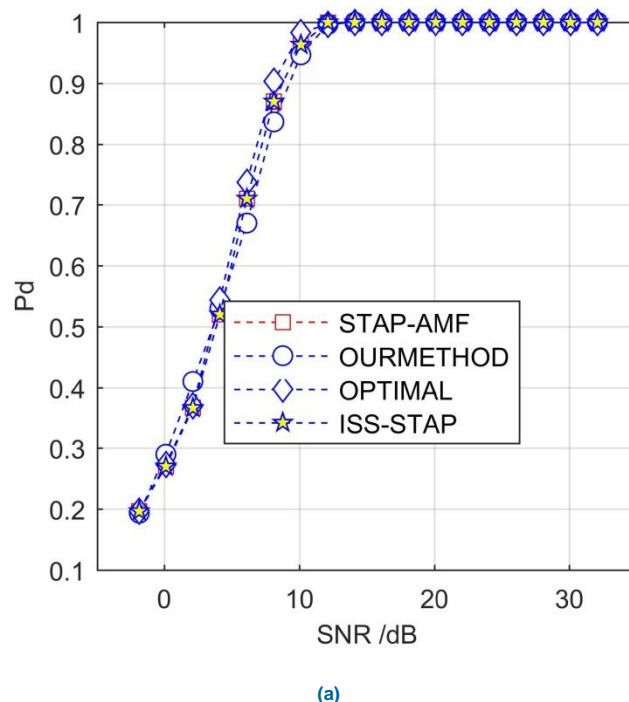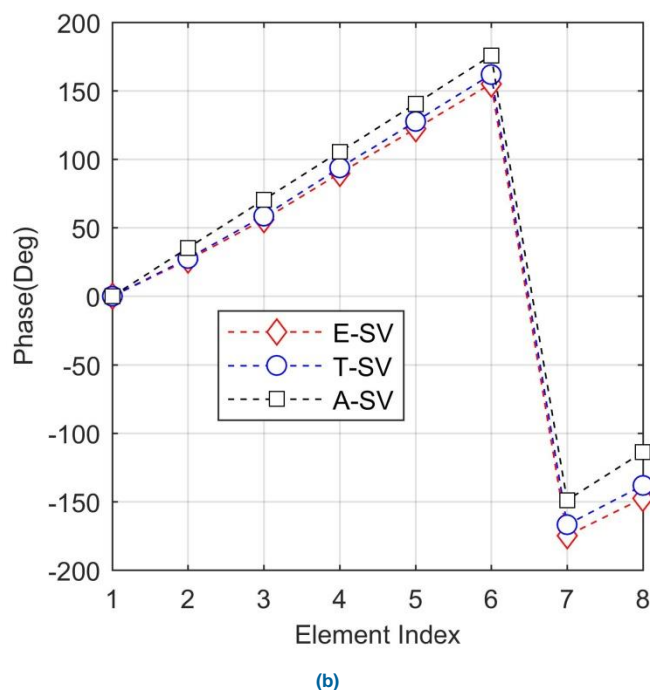

(b)

(a)

(c)

(b)

FIGURE 5. Performance comparison on steering vector estimation. (a) Amplitude, (b) Phase. E-SV denotes the estimated steering vector, T-SV denotes the true steering vector, and A-SV denotes the assumed steering vector.

B. DETECTION PERFORMANCE

In this example, the detection performance of the presented method (RSUBSPACE-STAP), the STAP-AMF detector[1] and the optimal detector given in [1], and the ISS-STAP method given in [4] are compared. The optimal detector is unavailable in real situations since it is assumed that the clairvoyant covariance matrix and the actual target steering vector are known. Thus, the optimal detector is employed here only for providing a benchmark. The detection performance curves are yielded by averaging 10000 independent trials, where the false alarm rate is 10e-2. In Fig.6, the detection curves versus SNR are given, where the array error is 10%, and the target angle is 0° and 5° relative to the look direction, respectively. It is shown that the presented method can obtain better detection performance than the STAP-AMF detector and the ISS-STAP method for almost SNR cases when the target direction deviates from the look direction. Although the STAP-AMF detector and the ISS-STAP method can obtain the optimal performance when the target is located at the look direction, the presence of array errors degrades their performance and the performance of the two methods are slightly better than that of the presented method in this case.
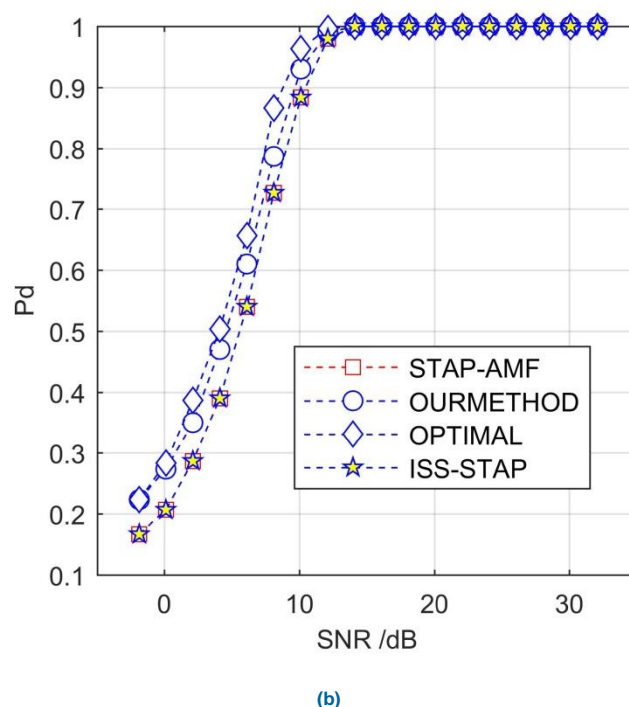

(a)

(b)

FIGURE 6. Detection curves versus SNR. (a) Target at the look direction, (b) target at 5° deviated from the look direction.

In Fig.7, the detection curves versus the target angle are given, where the array error is 10%, and the target SNR is 10.1dB. Relative to the STAP-AMF detector and the ISS-STAP detector, the presented method can obtain more robust detection performance in the mainbeam. It is shown that the presented method can obtain better performance at the edge of the beam, and has a slight performance loss in the center of the beam relative to the conventional AMF

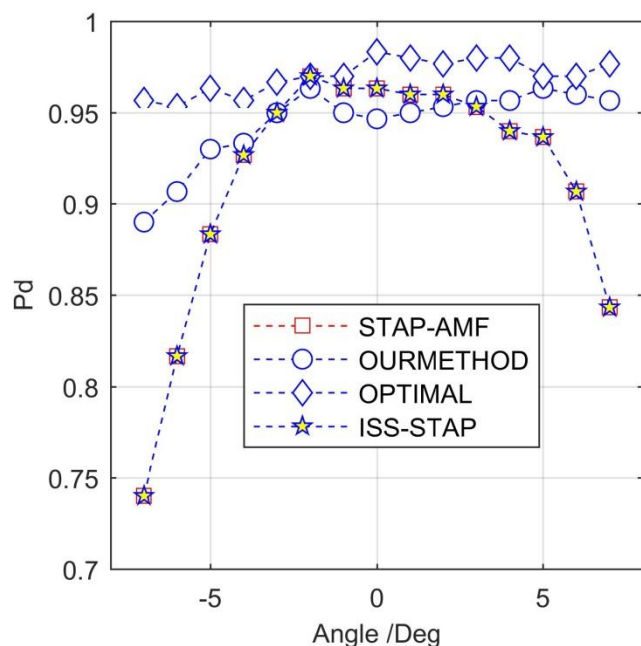detector due to the inherent property of the subspace detector.

FIGURE 7. Detection curves versus target angle.

C. ANGLE ESTIMATION PERFORMANCE

In this example, performance comparisons on angle estimation using three methods, including the presented method and the adaptive monopulse method and the ML method using assumed steering vectors, are made. The root mean squared error (RMSE) is employed to evaluate angle estimation performance, which is defined as

$$\text{RMSE}=\sqrt{\frac{1}{L}\sum_{l=1}^{L}\left(\hat{\theta}_{tl}-\theta_{t}\right)^{2}}$$, where $\hat{\theta}_{tl}$ is the target angle

estimate of the lth trial, θ_{t} is the true target angle and L is the number of independent trials. In Fig.8, the RMSEs of three methods as a function of target angle are given. It can be seen that the RMSE of the presented estimator can obtain better performance than the other methods. It lies in the fact that mismatched steering vectors result into incorrect cost function values and performance degradation.
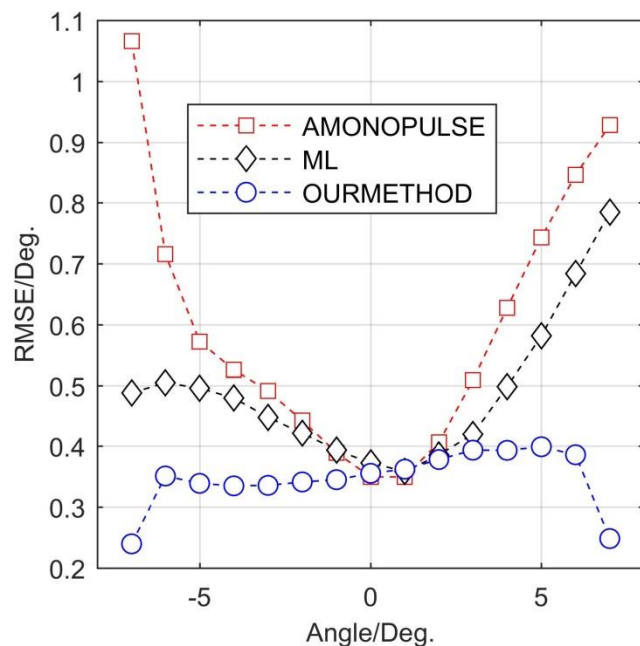

FIGURE 8. RMSE versus target angle.

V. CONCLUSIONS

The objective of this paper is to propose and evaluate the robust target detection and estimation method based on steering vector estimation and the subspace detector against steering vector mismatch resulted from array errors and target uncertainty. Utilizing the spatial-temporal coupling relationship of the ground clutter for an airborne radar, spatial steering vectors with arbitrary array errors can be well estimated by fined Doppler localization. Hereafter, the subspace detector based on estimated steering vectors are employed to reduce performance degradation induced by angle uncertainty and array errors. Finally, the reduced-dimensional ML angle estimator based on subspace coefficients derived from estimated steering vectors is developed.

REFERENCES
[1] R. Klemm, *Principles of space-time adaptive processing*, London, UK, The Institution of Electrical Engineers, 2002, pp.151-209.
[2] J. Ward, "Space-time adaptive processing for airborne radar," MIT Lincoln Lab., Lexington, MA, USA, Tech. Rep. 1015, Dec. 1994.
[3] K. Duan, H. Yuan, H. Xu, W. Liu and Y. Wang, "Sparsity-Based Non-Stationary Clutter Suppression Technique for Airborne Radar," *IEEE Access*, vol. 6, pp. 56162-56169, Oct. 2018.
[4] C. Duan, Y. Li, and W. W. Wang, "An intelligent sample selection method for space-time adaptive processing in heterogeneous environment", *IEEE Access*, vol.6, pp.26605-26616, Jun. 2018.
[5] W. Feng, Y. Guo, and X. He, "Joint iterative adaptive approach based space time adaptive processing using MIMO radar", *IEEE Access*, vol.8, pp.56162-56169, Oct. 2019.
[6] W. L. Shi, Y. S. Li, U. Y. Zhao and X. G. Liu, "Controllable sparse antenna array for adaptive beamforming," *IEEE Access*, vol. 7, pp. 6412-6423, Jan. 2019.
[7] B. P. Ng, J. P. Lie, M. H. Er and A. Feng, "A practical simple geometry and gain/phase calibration technique for antenna array processing," *IEEE Transactions on Antennas and Propagation*, vol. 57, no. 7, pp. 1963-1972, Jul. 2009.

[8] F. Q. Wen, Z. J. Zhang, K. Wang, G. Sheng and G. Zhang, "Angle estimation and mutual coupling self-calibration for ULA-based bistatic MIMO radar," *Signal processing*, vol. 144, pp. 61-67, Oct. 2017.

[9] C. Liu, Z. F. Ye, Y. F. Zhang, "Autocalibration algorithm for mutual coupling of planar array," *Signal processing*, vol. 90, no. 3, pp. 784-794, Aug. 2009.

[10] Z. Ma, Y. M. Liu, H. D. Meng, and X. Q. Wang, "Sparse recovery-based space-time adaptive processing with array error self-calibration," *Electronic Letters*, vol. 50, no. 13, pp. 152-154, Jun. 2014,

[11] Z. C. Yang, R. C. Lamare and W. J. Liu, "Sparsity-based STAP using alternating direction method with gain/phase errors," *IEEE Transactions on Aerospace and Electronic Systems*, vol. 53, no. 6, pp. 2756-2768, Dec. 2017.

[12] Y. Liu, B. Jiu and H. W. Liu, "Clutter-based gain and phase calibration for monostatic MIMO radar with partly calibrated array," *Signal processing*, vol. 158, pp. 219-226, Jan. 2019.

[13] X. W. Zhang, T. Jiang, Y. S. Li and Y. Zakharov, "A novel block sparse reconstruction method for DOA estimation with unknown mutual coupling," *IEEE Communications Letters*, vol. 23, no. 10, pp. 1845-1848, Oct. 2019.

[14] R. Goossens and H. Rogier, "A hybrid UCA-RARE/Root-MUSIC approach for 2-D direction of arrival estimation in uniform circular arrays in the presence of mutual coupling," *IEEE Transactions on Antennas and Propagation*, vol. 55, no. 3, pp. 841-849, Mar. 2007.

[15] A. D. Maio, "Robust adaptive radar detection in the presence of steering vector mismatches," *IEEE Transactions on Aerospace and Electronic Systems*, vol. 41, no. 4, pp. 1322-1337, Oct. 2005.

[16] F. Bandiera, A. D. Maio and G. Ricci, "Adaptive CFAR radar detection With conic rejection," *IEEE Transactions on Signal Processing*, vol. 55, no. 6, pp. 2533-2541, Jun. 2007.

[17] A. D. Maio, S. D. Nicola, Y. Huang, S. Zhang and A. Farina, "Adaptive detection and estimation in the presence of useful signal and interference mismatches," *IEEE Transactions on Signal Processing*, vol. 57, no. 2, pp. 436-450, Feb. 2009.

[18] A. D. Maio, S. D. Nicola and A. Farina, "GLRT versus MFLRT for adaptive CFAR radar detection with conic uncertainty," *IEEE Signal Processing Letters*, vol. 16, no. 8, pp. 707-710, Aug. 2009.

[19] A. D. Maio, Y. W. Huang, D. P. Palomar, S. Z. Zhang and A. Farina, "Fractional QCQP with applications in ML steering direction estimation for radar detection," *IEEE Transactions on Signal Processing*, vol. 59, no. 1, pp. 172-185, Jan. 2011.

[20] A. D. Maio and Y. W. Huang, "New results on fractional QCQP with applications to radar steering direction estimation," *IEEE Signal Processing Letters*, vol. 21, no. 7, pp. 895-898, Jul. 2014.

[21] J. X. Wu, T. Wang and Z. Bao, "Fast realization of maximum likelihood angle estimation in jamming: Further results," *IEEE Transactions on Aerospace and Electronic Systems*, vol. 50, no. 2, pp. 1556-1562, Apr. 2014.

[22] U. Nickel, "Overview of generalized monopulse estimation," *IEEE Aerospace and Electronic Systems Magazine*, vol. 21, no. 6, pp. 27-56, Jun. 2006.

[23] F. C. Robey, D. R. Fuhrmann, E. J. Kelly, R. Nitzberg, "A CFAR adaptive matched filter detector," *IEEE Transactions on Aerospace and Electronic Systems*, vol. 28, no. 1, pp. 208-216, Feb. 1992.

[24] K. Gerlach, S. D. Blunt and M. L. Picciolo, "Robust adaptive matched filtering using the FRACTA algorithm," *IEEE Transactions on Aerospace and Electronic Systems*, vol. 40, no. 3, pp. 929-945, Jul. 2004.

[25] O. Besson, L. L. Scharf and F. Vincent, "Matched direction detectors and estimators for array processing with subspace steering vector uncertainties," *IEEE Transactions on Signal Processing*, vol. 53, no. 12, pp. 4453-4463, Dec. 2005.

[26] W. Liu, J. Liu, L. Huang, K. Yan, Y. Wang, "Robust GLRT approaches to signal detection in the presence of spatial-temporal uncertainty," *Signal Processing*, vol. 118, pp. 272-284, Jun. 2015.
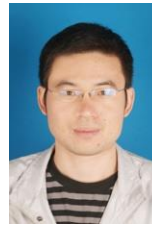
JIANXIN WU received the B.E. and Ph.D. degrees in signal processing from the Xidian University, Xi'an, China, in 2003 and 2009, respectively. He is currently an associate professor in the school of Electronics and Communication Engineering, Sun Yat-Sen University. His research interests include direction-of-arrival (DOA) estimation and space-time adaptive processing (STAP). Email: wujx65@mail.sysu.edu.cn

YANG ZHAO received a bachelor's degree from Northwest University in 2018 and currently pursuing for a master's degree in Electronic Communication Engineering at Xidian University. Her research direction is array signal processing.

CHANGXIAN LI received his master's degree from Xidian university in 2019 and his bachelor's degree from Xidian university in 2016. His research interest includes distributed radar clutter modeling and space-time adaptive processing.

PENG SHEN received the bachelor's degree in Electronic Information Engineering from Xidian university in 2017.He is currently pursuing the master's degree in Electronic Communication Engineering at Xidian university. His research direction is array signal processing.
[27]